MRS Communications (2017), 7, 873–878

doi:10.1557/mrc.2017.108

MRS Communications

Research Letter

Impact of enhanced oxide reducibility on rates of solar-driven thermochemical fuel production

Michael J. Ignatowich, Department of Chemical Engineering, California Institute of Technology, Pasadena, CA 91125, USA
Alexander H. Bork, ETH Zürich, Zürich 8093, Switzerland
Timothy C. Davenport, Department of Materials Science, Northwestern University, Evanston, IL 60208, USA
Jennifer L. M. Rupp, Department of Materials Science and Engineering, Massachusetts Institute of Technology, Cambridge, MA 02139, USA
Chih-kai Yang, Materials Science, California Institute of Technology, Pasadena, CA 91125, USA
Yoshihiro Yamazaki, INAMORI Frontier Research Center, Kyushu University, Fukuoka 819-0395, Japan
Sossina M. Haile, Department of Materials Science, Northwestern University, Evanston, IL 60208, USA; Materials Science, California Institute of Technology, Pasadena, CA 91125, USA

Address all correspondence to S. M. Haile at **sossina.haile@northwestern.edu**

(Received 12 August 2017; accepted 25 September 2017)

Abstract

Two-step, solar-driven thermochemical fuel production offers the potential of efficient conversion of solar energy into dispatchable chemical fuel. Success relies on the availability of materials that readily undergo redox reactions in response to changes in environmental conditions. Those with a low enthalpy of reduction can typically be reduced at moderate temperatures, important for practical operation. However, easy reducibility has often been accompanied by surprisingly poor fuel production kinetics. Using the $La_{1-x}Sr_xMnO_3$ series of perovskites as an example, we show that poor fuel production rates are a direct consequence of the diminished enthalpy. Thus, material development efforts will need to balance the countering thermodynamic influences of reduction enthalpy on fuel production capacity and fuel production rate.

Fuel production by two-step solar-driven thermochemical cycling (STC) has received significant attention as a means of storing solar energy.[1–3] Non-stoichiometric oxides, in combination with a temperature swing cycle, Fig. 1, have proven to be especially effective for this process.[4,5] Here, in a first step, thermal reduction of the oxide is carried out at high temperature, typically 1200–1500 °C (T_{TR}). Subsequent oxidation by steam and/or carbon dioxide at a lower temperature, typically 800–1000 °C (T_{FP}), generates the product fuel. While oxides of the fluorite structure-type (ceria and its doped derivatives) were the first, explicitly nonstoichiometric oxides evaluated for STC fuel generation,[6] perovskite-structured materials have emerged as attractive alternatives because of the possibility of lowering cycling temperatures.[7,8] In particular, decreasing the thermal reduction temperature from ∼1500 °C as required for reasonable efficiency from undoped ceria would significantly ease reactor design constraints and minimize solar re-radiation losses.[7]

The technological motivation for identifying an STC material with decreased thermal demands in combination with the compositional flexibility of perovskites has led to a surge of redox cycling studies in this material class.[8–16] A large majority of these efforts have focused on one key metric, fuel produced per cycle per unit mass (or mole) of oxide, i.e., fuel productivity. For oxidation by 20–40% steam values as high as 400 $\mu mol_{H_2}/g_{oxide}$ for $La_{0.5}Sr_{0.5}MnO_{3-\delta}$ (T_{TR} = 1400 °C/T_{FP} = 800 °C)[9] and 307 $\mu mol_{H_2}/g_{oxide}$ for $La_{0.6}Sr_{0.4}Mn_{0.6}Al_{0.4}O_{3-\delta}$ (T_{TR} = 1350 °C/T_{FP} = 1000 °C)[8] have been obtained. In contrast, for ceria, the expected fuel productivity for an equilibrium cycle with T_{TR} = 1350 °C/T_{TR} = 800 °C is just 128 $\mu mol_{H_2}/g_{oxide}$.[5,17] For oxidation by CO_2, perovskites appear to provide even larger fuel productivities than the attractive values obtained for hydrogen production. However, because fuel productivity in such cases is often estimated from mass gain on exposure to CO_2 and, as reported for the example of $(Ca,Sr)(La,Mn)O_{3-\delta}$, mass gain can occur due to carbonate formation,[11] such results must be viewed with some caution.

While productivity is an important criterion for identifying a desirable STC material, the rate at which the fuel is produced is equally important. To date, there have been few systematic studies of oxidation rates for perovskites, although some authors have noted sluggish kinetics relative to ceria.[18] Using as a metric the peak rate of fuel production in a fuel evolution profile, typical values in the range 0.06–0.50 $mL_{fuel}/min/g_{oxide}$ are evident in the perovskite literature. In contrast, peak fuel production rates as high as 12.5 $mL_{H_2}/min/g_{oxide}$[5] and even 60 $mL_{CO}/min/g_{oxide}$[19] have been obtained from ceria. While direct comparisons are not entirely meaningful without complete knowledge of the details of the experimental cycling conditions, these differences are extreme. Furthermore, while the oxidation reaction reaches completion within just a few

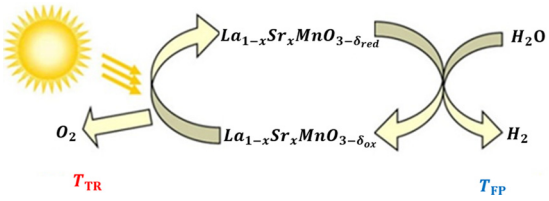

Figure 1. A thermochemical cycle that converts H_2O to H_2 by cyclic reduction and oxidation of a lanthanum strontium manganite oxide at respective temperatures T_{TR} (thermal reduction temperature) and T_{FP} (fuel production temperature) using solar-derived thermal energy as the input.

minutes for ceria, perovskites often require as much as 2 h or more to attain an equivalent extent of reaction.[9] The question immediately arises then whether there is a fundamental difference between the fluorite-structured and perovskite-structured classes of oxides that is responsible for this more than an order of magnitude difference in rates. We show here that the low fuel production rates observed in previous studies of $La_{1-x}Sr_xMnO_{3-\delta}$ (LSM) perovskites in particular are largely a consequence of the *thermodynamic* properties of the oxides rather than their *kinetic* properties. Because of the thermodynamic similarities between redox active perovskites, such limitations are likely to explain the behavior of many in this class.

Fundamental to the behavior of an STC material are the thermodynamic functions, the entropy and enthalpy, of the reduction reaction. In the limit of infinite material and infinitesimal changes in oxygen nonstoichiometry (ε) this reaction is expressed as

$$\lim_{\varepsilon\to 0}\frac{1}{\varepsilon}\mathrm{La}_{1-x}\mathrm{Sr}_x\mathrm{MnO}_{3-\delta} \Leftrightarrow \frac{1}{\varepsilon}\mathrm{La}_{1-x}\mathrm{Sr}_x\mathrm{MnO}_{3-\delta-\varepsilon}+\frac{1}{2}\mathrm{O}_2, \quad (1)$$

with equilibrium constant

$$K_{\mathrm{red}} = e^{-\Delta_{\mathrm{red}}G^0/RT} = \exp\left[\frac{T\Delta_{\mathrm{red}}S^0(\delta)-\Delta_{\mathrm{red}}H^0(\delta)}{RT}\right] = \hat{P}_{\mathrm{O}_2}^{\frac{1}{2}}(\delta, T). \quad (2)$$

Here, R is the universal gas constant, T is temperature, and $\Delta_{\mathrm{red}}G^0$, $\Delta_{\mathrm{red}}S^0(\delta)$, and $\Delta_{\mathrm{red}}H^0(\delta)$ are, respectively, the standard Gibbs energy, the standard entropy and the standard enthalpy of the reduction reaction, each of which depends on oxygen nonstoichiometry, δ. $\hat{P}_{\mathrm{O}_2}(\delta, T)$ is $P_{\mathrm{O}_2}(\delta, T)/P_{\mathrm{ref}}$, where $P_{\mathrm{O}_2}(\delta, T)$ is the oxygen partial pressure at equilibrium with the solid at a nonstoichiometry of δ. It is perhaps immediately obvious that knowledge of $\Delta_{\mathrm{red}}S^0(\delta)$, and $\Delta_{\mathrm{red}}H^0(\delta)$ allows one to directly compute the equilibrium fuel productivity for any given cycle spanning two thermodynamically defined endpoints. Less obvious is the connection between these thermodynamic quantities and the fuel production profile.

In recent works, we have shown that for a material with sufficiently high surface reaction coefficient and bulk diffusion coefficient, the rate at which fuel is produced from the reaction of the reduced oxide with the oxidant gas is dictated by the rate at which the gas is supplied to the material and the relative oxidizing capacity of that gas.[20,21] Under conditions in which (i) the gas fully interacts with the solid, (ii) the solid has a spatially uniform nonstoichiometry at any given time, (iii) the gas has a spatially uniform composition within the reaction zone, immediately equilibrating with the solid, and (iv) the product gases are in equilibrium with respect to thermolysis, the hydrogen evolution profile can be obtained from simple mass balance considerations. The result is[22]

$$\dot{\nu}_{\mathrm{H}_2} = -\dot{\nu}_{\mathrm{ox}}\left(\frac{(2\,P_{\mathrm{O}_2}(\delta, T_{\mathrm{FP}}))}{(P_{\mathrm{tot}}-P_{\mathrm{O}_2}(\delta, T_{\mathrm{FP}}))}-\frac{(\chi_{\mathrm{H_2O}}K_{\mathrm{H_2O},T})}{(\hat{P}_{\mathrm{O}_2}(\delta, T_{\mathrm{FP}})^{1/2}+K_{\mathrm{H_2O},T})}\right), \quad (3)$$

where $\dot{\nu}_{\mathrm{H}_2}$ is the oxide-mass-normalized volumetric flow rate of generated hydrogen (i.e., volumetric flow rate per unit mass of oxide), $\dot{\nu}_{\mathrm{ox}}$ is the oxide-mass-normalized inlet volumetric flow rate of oxidizing gas (comprising a mixture of steam and inert gas), $\chi_{\mathrm{H_2O}}$ is the mole fraction of steam in the oxidizing gas, $K_{\mathrm{H_2O},T}$ is the equilibrium constant for water thermolysis, at the temperature of fuel production, T_{FP}, and P_{tot} is the total system pressure, equal to 1 atm for a non-pressurized system. The oxygen partial pressure $\hat{P}_{\mathrm{O}_2}(\delta, T_{\mathrm{FP}})$, is that which is in equilibrium with the solid at any given instant, and evolves with time as the reaction proceeds. Under this formalism, an initial volume of gas enters the reactor and instantaneously equilibrates with the oxide. This instantaneous equilibration implies that the gas oxygen partial pressure decreases slightly and the oxygen content in the oxide increases slightly, such that the oxygen chemical potentials in the two phases equalize. The exiting gas is in equilibrium with the solid, and no further reaction takes place until the next volume of gas enters the reactor volume. From knowledge of the process parameters (T_{FP}, $\chi_{\mathrm{H_2O}}$, inlet gas flow rate, and mass of oxide), and the material thermodynamics of Eq. (2), it is possible *via* an iterative calculation to compute the hydrogen evolution profile, $\dot{\nu}_{\mathrm{H}_2}(t)$, where t is time.

Amongst perovskites considered for STC applications, the LSM series is unique in that the thermodynamic properties have been established with high reliability, and the hydrogen evolution profiles have been measured quantitatively under controlled thermodynamic conditions. In particular, in a previous study we reported $\Delta_{\mathrm{red}}S^0(\delta)$, and $\Delta_{\mathrm{red}}H^0(\delta)$ for $La_{0.8}Sr_{0.2}$ $MnO_{3-\delta}$ (LSM82), $La_{0.7}Sr_{0.3}MnO_{3-\delta}$ (LSM73), and $La_{0.6}Sr_{0.4}$ $MnO_{3-\delta}$ (LSM64) using $\delta(P_{\mathrm{O}_2}, T)$ data generated on the basis of earlier CALPHAD modeling of the LSM class of materials from Grundy et al.[23,24] The results were validated against more recent thermogravimetric measurements of LSM64.[15] We apply the same analysis methodology here of extracting thermodynamic parameters from CALPHAD computed nonstoichiometry data to $La_{0.9}Sr_{0.1}MnO_{3-\delta}$ (LSM91). The complete set of results, somewhat updated in the case of LSM82, LSM73 and LSM64 using slightly refined interpolation procedures, is presented in Fig. 2. A clear decrease in the magnitude of the enthalpy of reduction with increasing Sr content is evident, a feature noted in previous studies[9,16,24,25] and one that results in the increased reducibility of the Sr-rich compositions. The

https://doi.org/10.1557/mrc.2017.108

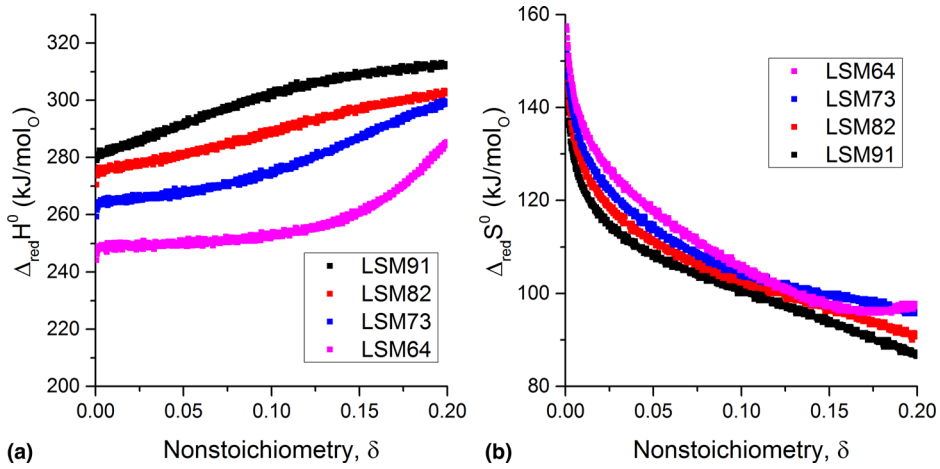

Figure 2. CALPHAD derived (a) enthalpy and (b) entropy of reduction of $La_{1-x}Sr_xMnO_{3-\delta}$ (LSM) compounds with strontium content from $x = 0.1$ (LSM91) to $x = 0.4$ (LSM64) each as a function of oxygen nonstoichiometry.

associated oxygen nonstoichiometry curves, Fig. 3, shown for 800 and 1400 °C, also reflect this increased reducibility.

The experimental hydrogen evolution profiles were obtained, as reported earlier, upon reduction at ~1400 °C under 10 ppm O_2 in flowing Ar, followed by oxidation at ~800 °C under 20% steam (balanced by Ar).[9] The non-stoichiometry values resulting from the reduction step are indicated in Fig. 3(a), and the strong increase in oxygen loss with increasing with Sr content is clear. As a result of the rapid quench from high temperature, these non-stoichiometries correspond to the values, δ_i, at the initiation of the oxidation reaction. Oxidation then occurs in accordance with the low temperature oxygen nonstoichiometry curves, Fig. 3(b). Due to anticipated kinetic challenges with the creation of material volume to accommodate oxygen nonstoichiometry in the oxygen excess region, oxygen content beyond 3 is not considered here. A comparison of experimental and computed profiles, Fig. 4, shows that, with the exception of the very short time results (at which gas mixing effects impact the measured profiles[21]), good agreement is obtained, particularly for LSM91 and LSM82. We note that due to uncertainty in the exact sample temperature in the IR imaging furnace employed for the experimental studies, both reduction and oxidation temperatures were slightly adjusted, Table I, to achieve the level of agreement evident in Fig. 4. Regardless of this detail, it is clear that enhanced reducibility with increasing Sr content directly translates into a decrease in fuel production rates. For LSM91 and LSM82, the rates appear entirely limited by this thermodynamic effect. For LSM73 and LSM64, an additional material-kinetic effect, likely a surface reaction limitation,

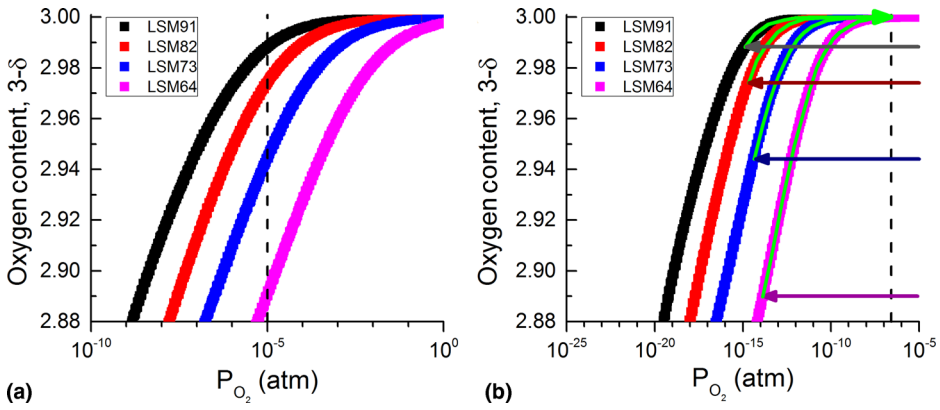

Figure 3. Oxygen content in LSM compounds as a function of oxygen partial pressure at (a) 1400 °C and (b) 800 °C. Reduction under 10^{-5} atm O_2 is indicated by the vertical line in (a). Upon quenching from the reduction condition to 800 °C, the materials retain the δ attained at high temperature, implying an internal chemical potential corresponding to the intersection of the horizontal δ_i lines in (b) with the 800 °C curves. The vertical line in (b) is the equilibrium oxygen partial pressure resulting from thermolysis of 20% H_2O in Ar, used experimentally for the fuel production half-cycle. The thermodynamic driving force for the initiation of the oxidation reaction is determined by the distance between the vertical line in (b) and the nonstoichiometry curve at δ_i.

https://doi.org/10.1557/mrc.2017.108

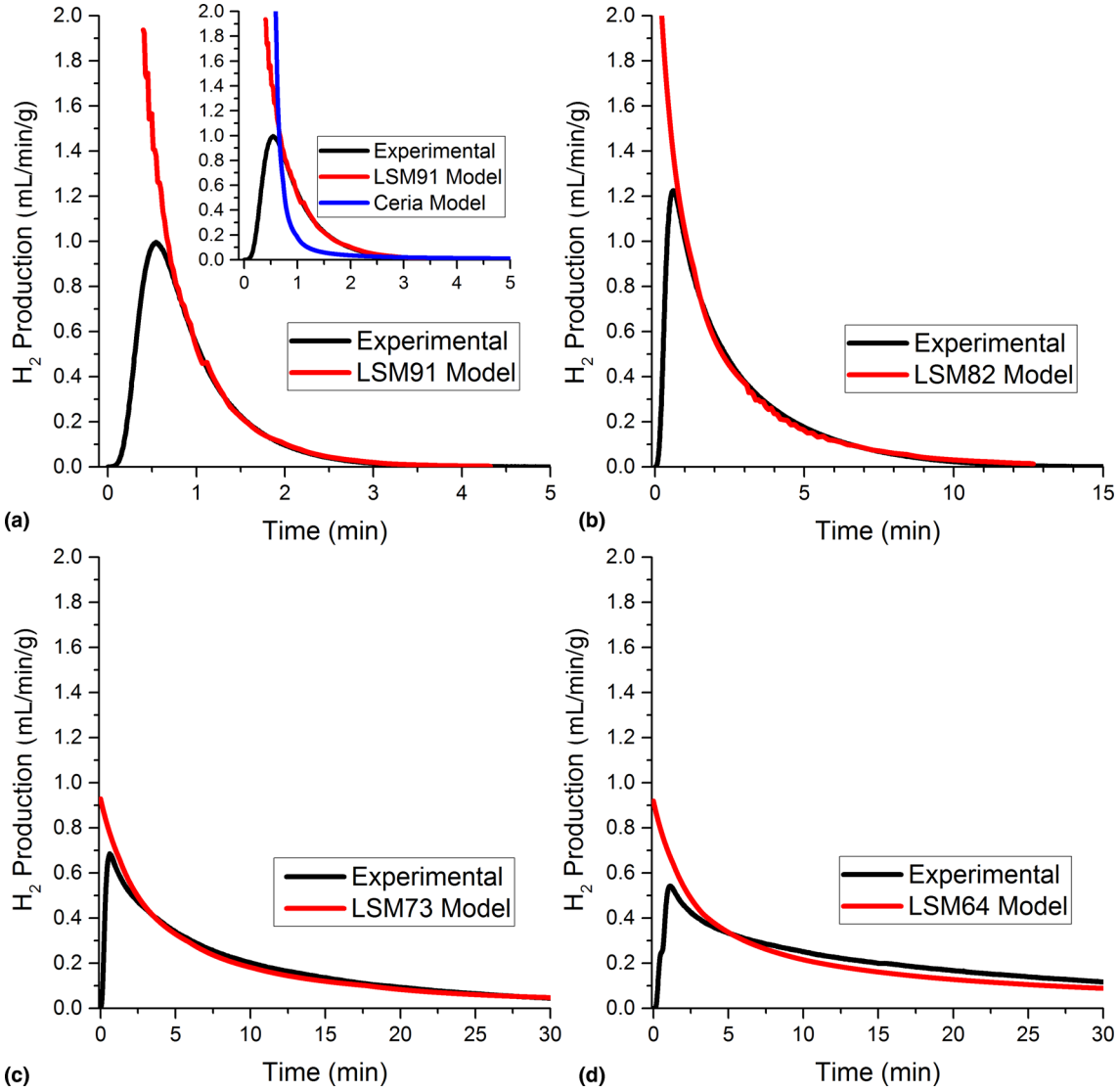

Figure 4. Hydrogen production calculated by the thermo-kinetic (quasi-equilibrium) model compared to experimental data for two temperature cycling of LSM compounds: (a) LSM91, (b) LSM82, (c) LSM73, and (d) LSM64. Reduction performed nominally at 1400 °C under 10 ppm O_2, and oxidation nominally at 800 °C under 20% steam at 200 mL/min. The inset in (a) additionally shows the computed behavior of ceria in the thermokinetic limit. Experimental data have been reported previously and reflect the hydrogen detected by mass spectrometry in the evolved gas stream.[9]

appears to play a role. These two compositions underperform the model for a short period just beyond the peak in the hydrogen evolution profiles (beyond which the effects of gas mixing are negligible), and subsequently produce hydrogen for a much longer period than predicted by the thermochemical model.

The slow rates of hydrogen generation with increasing Sr content can be understood by directly considering the oxygen nonstoichiometry profiles, Fig. 3(a). The total driving force for oxidation is effectively the difference between $P_{O_2}(\delta_i, T_{FP})$, the oxygen partial pressure which would be in equilibrium with the quenched nonstoichiometry from the high-temperature reduction, $\delta(P_{O_2} = 10^{-5}$ atm, $T = 1400\,°C)$, and the oxygen partial pressure of the inlet steam, 1.6×10^{-7} atm. This difference systematically decreases with increasing Sr, although the total $\Delta\delta$ between oxidized and reduced conditions systematically increases. The fact that $P_{O_2}(\delta_i, T_{FP})$ is relatively high for LSM64 is a direct consequence of the thermodynamic ease by which reduction of this material occurs. The diminished $\Delta_{red}H^0(\delta)$ at high Sr content with relatively unchanging $\Delta_{red}S^0(\delta)$ implies a diminished driving force for oxidation at all temperatures. Decoupling the high and low temperature responses, as dictated by $\Delta_{red}G^0(\delta) = \Delta_{red}H^0(\delta) - T\Delta_{red}S^0(\delta)$, would require manipulation of $\Delta_{red}S^0(\delta)$. The benefit of designing materials with large $\Delta_{red}S^0(\delta)$ in the context of increasing fuel *productivity* (quantity of fuel per unit oxide per equilibrium cycle) has been

https://doi.org/10.1557/mrc.2017.108

Table I. Process parameters for the computation of thermo-kinetic hydrogen production profiles.

Material	Mass (mg)	T_{TR} (°C)	δ_i	T_{FP} (°C)	$\dot{v}_{ox}$ (sccm/g_{oxide})	$\dot{v}_{H_2}^{max,\ computed}$ (sccm/g_{oxide})
LSM91	490	1385	0.01	840	408	5.99
LSM82	540	1440	0.04	795	370	2.70
LSM73	530	1440	0.07	810	377	0.929
LSM64	510	1400	0.13	800	392	0.919
Ceria[a]	490	1385	0.03	840	408	50.4

Experimentally, reduction of LSM was carried out at 1400 ± 40 °C under flow of 10^{-5} atm O_2 in Ar. The 40 min reduction period was sufficient to achieve equilibration. Fuel production was carried out at 800 ± 40 °C under flow of 0.2 atm H_2O in Ar, provided at a flow rate of 200 mL/min.
[a]Cycling conditions are selected to match those of LSM91.

previously discussed in the literature.[26] Here it is evident that the benefits extend to fuel production *rates* (fuel per unit oxide per unit time). To put the magnitude of the latter effect into context, we note that for all LSM compositions, the computed peak production rates for the quasi-equilibrium model fall below 3 $mL_{H_2}/min/g_{oxide}$. In contrast, for ceria reduced and oxidized under similar conditions the computed peak rate is almost 60 $mL_{H_2}/min/g_{oxide}$, although material kinetic effects (i.e., finite surface reaction rates) have precluded observation of this extremely high value for hydrogen production.[21] Increasing the fuel production rate from LSM to values comparable with those achieved from ceria could, in principle, be achieved by increasing the reactant gas flow rate, but an order of magnitude increase would be impractical. Given this reality, design of reactors making use of materials with low thermodynamic driving force for oxidation would have to address their inherently low fuel production rates.

Acknowledgments

Support for this work was provided in part by the US Department of Energy, ARPA-e HEATS program (DE-AR0000182), under subcontract from the University of Minnesota.

References

1. T. Kodama and N. Gokon: Thermochemical cycles for high-temperature solar hydrogen production. *Chem. Rev.* **107**, 4048 (2007).
2. M. Romero and A. Steinfeld: Concentrating solar thermal power and thermochemical fuels. *Energy Environ. Sci.* **5**, 9234 (2012).
3. C. Agrafiotis, M. Roeb, and C. Sattler: A review on solar thermal syngas production via redox pair-based water/carbon dioxide splitting thermochemical cycles. *Renew. Sustainable Energy Rev.* **42**, 254 (2015).
4. W.C. Chueh, C. Falter, M. Abbott, D. Scipio, P. Furler, S.M. Haile, and A. Steinfeld: High-Flux Solar-Driven Thermochemical Dissociation of CO_2 and H_2O Using Nonstoichiometric Ceria. *Science* **330**, 1797 (2010).
5. W.C. Chueh and S.M. Haile: A thermochemical study of ceria: exploiting an old material for new modes of energy conversion and CO_2 mitigation. *Philos. Trans. R. Soc. London, Ser. A* **368**, 3269 (2010).
6. W.C. Chueh and S.M. Haile: Ceria as a thermochemical reaction medium for selectively generating syngas or methane from H_2O and CO_2. *ChemSusChem* **2**, 735 (2009).
7. J.R. Scheffe, D. Weibel, and A. Steinfeld: Lanthanum–strontium–manganese perovskites as redox materials for solar thermochemical splitting of H_2O and CO_2. *Energy & Fuels* **27**, 4250 (2013).
8. A.H. McDaniel, E.C. Miller, D. Arifin, A. Ambrosini, E.N. Coker, R. O'Hayre, W.C. Chueh, and J.H. Tong: Sr- and Mn-doped $LaAlO_{3-\delta}$ for solar thermochemical H_2 and CO production. *Energy Environ. Sci.* **6**, 2424 (2013).
9. C.-K. Yang, Y. Yamazaki, A. Aydin, and S.M. Haile: Thermodynamic and kinetic assessments of strontium-doped lanthanum manganite perovskites for two-step thermochemical water splitting. *J. Mater. Chem. A* **2**, 13612 (2014).
10. A.H. Bork, M. Kubicek, M. Struzik, and J.L.M. Rupp: Perovskite $La_{0.6}Sr_{0.4}Cr_{1-x}Co_xO_{3-\delta}$ solid solutions for solar-thermochemical fuel production: strategies to lower the operation temperature. *J. Mater. Chem. A* **3**, 15546 (2015).
11. M.E. Galvez, R. Jacot, J. Scheffe, T. Cooper, G. Patzke, and A. Steinfeld: Physico-chemical changes in Ca, Sr and Al-doped La-Mn-O perovskites upon thermochemical splitting of CO_2 via redox cycling. *Phys. Chem. Chem. Phys.* **17**, 6629 (2015).
12. S. Dey and C.N.R. Rao: Splitting of CO_2 by manganite perovskites to generate CO by solar isothermal redox cycling. *ACS Energy Lett.* **1**, 237 (2016).
13. Z.K. Zhang, L. Andre, and S. Abanades: Experimental assessment of oxygen exchange capacity and thermochemical redox cycle behavior of Ba and Sr series perovskites for solar energy storage. *Sol. Energy* **134**, 494 (2016).
14. T. Cooper, J.R. Scheffe, M.E. Galvez, R. Jacot, G. Patzke, and A. Steinfeld: Lanthanum manganite perovskites with Ca/Sr A-site and Al B-site doping as effective oxygen exchange materials for solar thermochemical fuel production. *Energy Tech.* **3**, 1130 (2015).
15. M. Takacs, M. Hoes, M. Caduff, T. Cooper, J.R. Scheffe, and A. Steinfeld: Oxygen nonstoichiometry, defect equilibria, and thermodynamic characterization of $LaMnO_3$ perovskites with Ca/Sr A-site and Al B-site doping. *Acta Mater.*. **103**, 700 (2016).
16. A.H. Bork, E. Povoden-Karadeniz, and J.L.M. Rupp: Modeling thermochemical solar-to-fuel conversion: CALPHAD for thermodynamic assessment studies of perovskites, exemplified for $(La,Sr)MnO_3$. *Adv. Energy Mater.* **7**, 1601086 (2017).
17. R.J. Panlener, R.N. Blumenthal, and J.E. Garnier: Thermodynamic study of nonstoichiometric cerium dioxide. *J. Phys. Chem. Solids* **36**, 1213 (1975).
18. A. Demont, S. Abanades, and E. Beche: Investigation of perovskite structures as oxygen-exchange redox materials for hydrogen production from thermochemical two-step water-splitting cycles. *J. Phys. Chem. C* **118**, 12682 (2014).
19. L.J. Venstrom, R.M. De Smith, R.B. Chandran, D.B. Boman, P.T. Krenzke, and J.H. Davidson: Applicability of an equilibrium model to predict the conversion of CO_2 to CO via the reduction and oxidation of a fixed bed of cerium dioxide. *Energy & Fuels* **29**, 8168 (2015).
20. T.C. Davenport, C.K. Yang, C.J. Kucharczyk, M.J. Ignatowich, and S.M. Haile: Implications of exceptional material kinetics on thermochemical fuel production rates. *Energy Tech.* **4**, 764 (2016).
21. T.C. Davenport, M. Kemei, M.J. Ignatowich, and S.M. Haile: Interplay of material thermodynamics and surface reaction rate on the kinetics of thermochemical hydrogen production. *Int. J. Hydrogen Energy* **42**, 16932 (2017).

https://doi.org/10.1557/mrc.2017.108

22. T.C. Davenport, C.K. Yang, C.J. Kucharczyk, M.J. Ignatowich, and S.M. Haile: Maximizing fuel production rates in isothermal solar thermochemical fuel production. *Appl. Energy* **183**, 1098 (2016).
23. A.N. Grundy, M. Chen, B. Hallstedt, and L.J. Gauckler: Assessment of the La–Mn–O system. *J. Phase Equil. Diff.* **26**, 131 (2005).
24. A.N. Grundy, E. Povoden, T. Ivas, and L.J. Gauckler: Calculation of defect chemistry using the CALPHAD approach. *Calphad Comp. Coupl. Ph. Diagr. Thermochem.* **30**, 33 (2006).
25. J. Mizusaki, N. Mori, H. Takai, Y. Yonemura, H. Minamiue, H. Tagawa, M. Dokiya, H. Inaba, K. Naraya, T. Sasamoto, and T. Hashimoto: Oxygen nonstoichiometry and defect equilibrium in the perovskite-type oxides $La_{1-x}Sr_xMnO_{3+\delta}$. *Solid State Ion.* **129**, 163 (2000).
26. B. Meredig and C. Wolverton: First-principles thermodynamic framework for the evaluation of thermochemical H_2O- or CO_2-splitting materials. *Phys. Rev. B* **80**, 245119 (2009).

https://doi.org/10.1557/mrc.2017.108